GT2024-122800

CENTRIFUGAL COMPRESSOR SURGE IN CLOSED LOOP SYSTEMS: INITIAL MODELLING AND COMPARISON WITH EXPERIMENTS

Sreenath Purushothaman
University of Genoa,
TPG, Genova, Italy

Federico Reggio
University of Genoa,
TPG, Genova, Italy

Alberto Traverso
University of Genoa,
TPG, Genova, Italy

Carlo Alberto Niccolini Marmont Du Haut Champ
University of Genoa,
TPG, Genova, Italy

Paolo Silvestri
University of Genoa,
TPG, Genova, Italy

Chaitanya Halbe
Carrier Corporation
Syracuse, NY

ABSTRACT

Heat pumps are expected to play a primary role in electrification of thermal users in the residential and industrial sectors. Dynamic compressors are widely used in large size heat pumps, thanks to their industrial replicability, compact size, affordable costs, and good performance in terms of efficiency and low acoustic emissions. The instability, which may occur in a compressor installed in closed loop cycle such as in a heat pump, is quite different from the classic open loop configuration involving dynamic compressors. This is mainly due to the complexity of the compressor instability mechanism coupled to a vapor compression system connected with two- phase heat exchangers, having different thermal and fluid dynamic capacitance properties, under a physical feedback loop.

The aim of this paper is to investigate the behavior of a dynamic compressor installed in an innovative heat pump prototype, of laboratory scale, under stable and unstable conditions. A preliminary simple dynamic model of the compression system consisting of a radial compressor, condenser and evaporator, is developed to represent the heat pump compression system, aiming at its time-dependent representation during compressor instable behavior. The evaporator and condenser are modelled using empirical correlations representing the heat exchange and phase change phenomena and including the thermal capacitances due to refrigerant mass and heat exchanger pipes. The preliminary validation of the dynamic model results is done through a dedicated experimental campaign, under different operating conditions. Results show the complexity of the interaction between the centrifugal compressor and the heat pump loop, discerning the different contributions to the time-dependent response of the system. Future steps will encompass a more detailed modelling of the heat pump loop and the use of updated field measurements, including liquid level meters in the heat exchangers.

Keywords: Surge modelling, heat pumps, closed loop cycles.

NOMENCLATURE

Symbols

A_{eq}	Compressor equivalent duct area [m^2]
C	Compressor pressure rise [Pa]
C_{SS}	Compressor steady-state characteristics [Pa]
C_v	Specific heat [J/kg K]
h	Enthalpy [J/kg]
L_{eq}	Compressor equivalent duct length [m]
m	Mass [kg]
$\dot{m}_{COMP}$	Compressor mass flow rate [kg/s]
$\dot{m}_{H2O}$	Water mass flow rate [kg/s]
N_R	Rotor revolutions [-]
P	Static Pressure [Pa]
P_t	Stagnation Pressure [Pa]
R	Refrigerant fluid
R_m	Mean rotor radius [m]
T	Temperature [K]
$T_{Ref\_sat.v}$	Saturated vapor temperature of refrigerant [K]
U_m	Mean rotor speed [m/s].
C_p^*	Pseudo specific heat [J/kg K]
$V_{effective}$	Effective liquid volume in the heat exchanger [m^3]
W	Water
ρ	Density [kg/m^3]
τ	Compressor time delay [s]

Abbreviations

ARL	Auxiliary Resistance Load
CV	Expansion valve
COMP	Compressor
COND	Condenser
FT	Flow transducer
EVA	Evaporator

1. INTRODUCTION

In the era of decarbonization, the production of heat through electric consumption is crucial to limit fossil fuel consumption. In the European Union, the residential sector consumes 25.4% of the energy use and contributes 20% of the greenhouse gas emissions [1,2]. As an alternative, heat pumps are expected to play a primary role in providing thermal power to the residential and industrial sectors. Therefore, it is important to find new solutions to increase the performance and enhance the operational range of the heat pumps, while reducing the maintenance and running costs.

Turbo heat pumps containing dynamic compressors circulates the refrigerant to produce the heat transfer effect with two heat exchangers [3]. These heat exchangers, condenser, and evaporator, use phase transition of the refrigerant from liquid to gas and vice versa. As in any compression system, these heat pumps are also susceptible to instability phenomenon such as stall and surge. But the complexity of the phenomena is different, as it involves peculiar traits such as closed loop system, placement of compressor between two plena (condenser and evaporator), real gas effects and the 2-phase nature of the fluid in the system [4,5]. The classical compressor surge models developed by Moore and Greitzer [6,7] for a simple open loop system is not suitable for these applications. Even though there have been advancements in the model to include closed loop cycles [8], the phase change and heat transfer phenomena are difficult to capture completely. Song et al. [3] and Kim and Song [5] have developed a model to capture the heat exchangers as well in recent years using detailed equations for phase change.

This paper describes the results of the initial attempts to develop a closed loop, 2-phase, compression system model for an innovative heat pump at the University of Genova, Italy [9,10]. The model is validated using experimental data from a dedicated compression system available at the Thermochemical Power Group, University of Genova. For studying unstable operation of refrigerant closed loop systems, Carrier Corporation provided the University of Genoa with a small size heat pump rig [9] equipped with a high-speed centrifugal compressor driven by a variable speed motor. The model comparison with experimental data was done using the closed loop innovative heat pump test rig available at the Thermochemical Power Group, University of Genova [9,10].

2. MODELLING METHODOLOGY

TRANSEO is a MATLAB-Simulink based simulation tool capable of transient and dynamic simulation of systems, developed by the Thermochemical Power Group, of the University of Genova, Italy. It is designed for simulating systems operating with different cycles and different sizes. It has been successfully employed in the study of microturbine-based energy systems [11,12], and hybrid fuel cell system [13] and for supercritical CO2 cycles [14]. The TRANSEO tool has over 30 built-in modules, along with standardized interconnecting protocols for assembling the modules to obtain the desired system layout. For the first time, TRANSEO modelling approach has been exploited for transient modelling of a two-phase system, such as the heat pump vapor compression test rig of this paper.

The compression system represented here is similar to the Moore-Greitzer compressor model [6,7], but includes two heat exchanger components that contain vapor mass flow source terms: the Evaporator, as vapor mass source, and the Condenser, as vapor mass sink. At the moment, these two components are represented, at steady state, by two empirical correlations simulating the heat transfer with the external heat transfer fluid, water in this case. Furthermore, they are dynamically characterized by their own energy conservation equations, explained in the following section, capturing their main thermal capacitances. At the moment, the effect of gas phase in these two components through plena components in between heat exchangers and the compressor is not modelled, since, by comparison with experiments, the results were sufficiently accurate already. However, this aspect is currently object of investigation for a more detailed model.

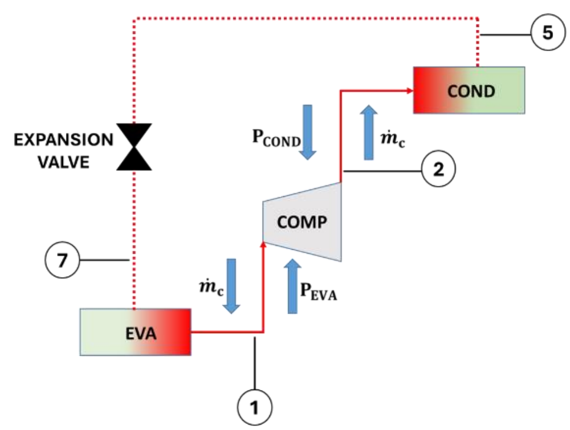

FIGURE 1: SCHEMATIC OF THE COMPRESSION SYSTEM

FIGURE 1 shows the schematic of the loop & modelling approach, where mass flow information is generated in the compressor model, through its momentum conservation equation, and is transferred to the two heat exchangers that, through two-phase energy balance equations, are capable of estimating their pressure value. The expansion valve in the physical system is not modelled in this approach, as its effect is included in the empirical relationships of the two heat exchangers.

FIGURE 2 shows a generic heat pump cycle in the p-h diagram. Point 8 corresponds to saturated vapor state in the evaporator, point 1 corresponds to compressor inlet, point 2 at compressor outlet, point 3 represents saturated vapor state in the condenser, point 4 is the saturated liquid state in condenser, point 5 corresponds to condenser exit, process 5 to 7 represents the process in the expansion valve and point 7 represents the two-phase state inside the evaporator.

In this paper, only the cycle from point 7 to point 5, in counterclockwise direction, is modelled. In fact, the mass continuity around the loop is not preserved. Even if this assumption sounds problematic, it is not for the purpose of this study. In fact, experiments show that the surge cycles occur at a pace much faster than the refrigerant replacement time in the heat exchangers (approximately 20% reduction in condenser liquid levels over 3 minutes). In other words, the fluctuations of mass flow through the compressor during surge in the short time do not significantly influence the liquid levels in the two heat exchangers, that behave as refrigerant fluid storages. So, during a limited number of surge cycles, it is possible to assume constant levels of liquid refrigerant in the evaporator and in the condenser.

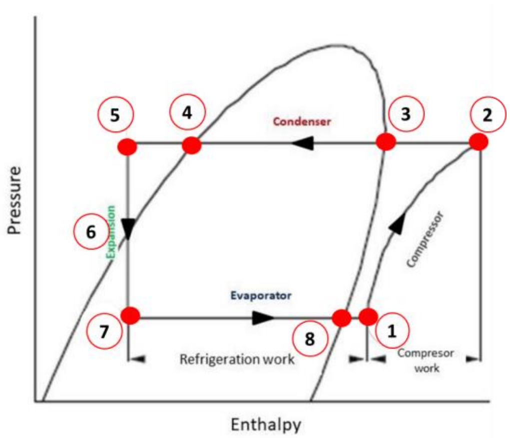

FIGURE 2: PRESSURE – ENTHALPY DIAGRAM FOR A TYPICAL HEAT PUMP SYSTEM.

2.1 Compressor modelling

According to the classical Moore-Greitzer model [6,7] the compressor is modelled as an actuator disk and an equivalent duct. The assumptions made by Greitzer for the compressor are used here as well, despite applied to a fluid with real gas behavior [15]:

1) The flow in equivalent ducts is considered incompressible.
2) Assuming that a given rate of change of mass flow produces the same unsteady pressure difference in the model as in the actual duct and matching the equivalent duct area to a characteristic area, an equivalent duct geometry can be determined.
3) When the stall limit is reached, and the flow field becomes unstable, there is a time lag between the onset of instability and the fully developed stall pattern.
4) This time is equal to or longer than the order of several rotor revolutions (N_R).
5) This time delay (τ) is employed in the way the compressor pressure rise (C) is calculated from the steady-state characteristics (C_{SS}).

Therefore, the governing equations in dimensional form for the compressor are as below.

$$\frac{d\dot{m}_{COMP}}{dt} = \left(\frac{A_{eq}}{L_{eq}}\right)(P_1 - P_2 + C) \tag{1}$$

$$\frac{dC}{dt} = \frac{(C_{SS} - C)}{\tau} \tag{2}$$

$$\tau = \frac{2\pi R_m N_R}{U_m} \tag{3}$$

2.2 Empirical correlation for Heat Exchanger model

The heat exchangers are modelled as simple volumes, which accept compressor mass flow information ($\dot{m}_C$) and use empirical correlations to provide the pressure information, P_1 on the evaporator outlet (state 1) and P_2 on the condenser inlet (state 2). In this work, as an initial attempt to capture the complex phenomena inside the condenser and evaporator, the heat transfer between the refrigerant and the external water supply is used to determine such pressures.

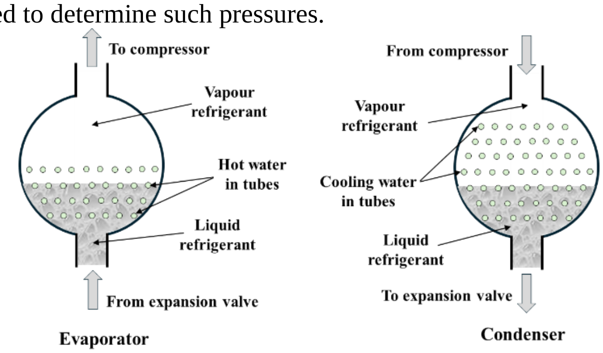

FIGURE 3: SHELL AND TUBE TYPE HEAT EXCHANGERS.

In the evaporator, the refrigerant enters in 2-phase condition (state 7 in FIGURE 2). The refrigerant then absorbs heat from the hot water supply from outside (FIGURE 3), which is the heat source, and undergoes phase transition into gaseous state at approximately constant pressure, till the saturation point (state 8). Further supply of heat to the refrigerant results in the sensible heating, termed as evaporator super heat, and reaches the compressor inlet condition (state 1) in gaseous form. Similarly, on the condenser side, the refrigerant leaves the compressor at state 2. The high-pressure refrigerant in gaseous form is cooled to saturated vapor state (state 3) and then phase transitioned into saturated liquid state (state 4) by the cooling water supply (FIGURE 3). Any further heat transfer with the cooling water results in condenser sub cooling (state 5), and the liquid refrigerant enters the expansion valve (states 5-7).

In order to capture these complex phenomena, the heat transfer between the external water supply and the refrigerant fluid are calculated for evaporator and condenser, using two empirical correlations tuned on experimental data at steady state conditions. First, a pseudo specific heat $C_p{}^*$ is calculated for each of the heat exchangers using enthalpy balance at the last stable point in the compressor characteristics curve (Eq. 4 & 5). Such pseudo specific heat would be exactly equal to the real cooling water specific heat in case the water outlet temperature would correspond to the refrigerant saturation temperature: such condition represents a good approximation of many experimental conditions.

$$C_p{}^*{}_{COND} = \frac{\dot{m}_{COMP}(h_2 - h_5)}{\dot{m}_{H2O}[T_{Ref\_sat.v,2} - T_{H2O,COND,in}]} \quad (4)$$

$$C_p{}^*{}_{EVA} = \frac{\dot{m}_{COMP}(h_1 - h_7)}{\dot{m}_{H2O}[T_{H2O,EVA,in} - T_{Ref\_sat.v,1}]} \quad (5)$$

These are then used in the energy conservation equations (Eq. 6 & 7) to estimate the thermal source term during transient operation, based on the external water supply and the current refrigerant saturation temperature, as shown below.

$$\frac{d(m_{EVA}\, C_{V,EVA}\, T_{EVA})}{dt} = \dot{m}_{H2O,EVA,in}\, C_p{}^*{}_{EVA}\left(T_{H2O,EVA,in} - T_{Ref\_sat.v,1}\right) - \dot{m}_{COMP}(h_1 - h_7) \quad (6)$$

$$\frac{d(m_{COND}\, \mathrm{C_{V,COND}}\, T_{COND})}{dt} = \dot{m}_{COMP}(h_2 - h_5) - \dot{m}_{H2O,COND,IN} C_p{}^*{}_{COND}(T_{Ref\_sat.v,2} - T_{H2O,COND,in}) \quad (7)$$

The mass of liquid inside the heat exchangers is calculated using the effective volumes of liquid inside the heat exchangers and the density of the liquid refrigerant at the corresponding saturated vapor states (Eq. 8 & 9). The effective volume corresponds to the net volume occupied by the refrigerant liquid, which is a function of the liquid level.

$$m_{EVA} = V_{effective,EVA} \times \rho_{7,liquid} \quad (8)$$

$$m_{COND} = V_{effective,COND} \times \rho_4 \quad (9)$$

The densities in equations (6) and (7) correspond to the liquid phase as the gas phase is not considered in this model. The differential equations (6) and (7) allow us to know, at each time step, the saturated liquid temperature of the refrigerant in the respective heat exchangers. The model responds to the saturated liquid temperature variations and the heat exchanger pressure is then estimated from the Pressure – Enthalpy diagram [15], assuming saturated conditions. This pressure is the same for both the liquid and the vapor states of refrigerant. As it can be seen from the formulation above, the thermal capacitance of refrigerant in the vapor phase, as well as its compressibility (i.e. mass storage effects through continuity equations) are not currently included in the model.

Furthermore, equations (8) and (9) would require knowledge about the refrigerant levels in the actual heat exchangers. This information was not reliably known at the time of model development. Therefore, based on experience & visual inspection of the heat exchangers, realistic assumptions regarding the liquid levels have been made, and fine tuning of liquid levels have been used to capture the experimental results. Detailed modelling with accurately measured refrigerant levels is planned for the next steps of this activity.

3. EXPERIMENTAL METHODOLOGY

The test rig consists of shell and tube type evaporator and condenser, a radial compressor, an expansion valve, a resistance heat load setup and the hot flow water supply to the evaporator, a cold flow water supply for the condenser, temperature measurement instruments (resistance type (Trafag – DIN 1/10 with 0.18 K uncertainty) and thermocouples (Type T with 0.9 K uncertainty)), pressure transducers (Setra – Pressure Transmitter 206 with 10 mbar uncertainty) and mass flow meters for the water circuits (FIP – F3.00 Paddlewheel sensor with maximum 3% relative uncertainty). Vibration measurements were performed by using an accelerometer on the compressor casing in axial direction. Acoustic noise measurements were performed with a high dynamic response pre-polarized microphone facing compressor casing.

	Value	Unit
Fluid	R1233zd-(E)	-
Max electric power	7.5	kW
Max pressure ratio	3.45	-
Max Compressor speed ($nmax$)	75	krpm
Compressor diffuser	vaned	-
Number of rotor blades	14	-
Number of splitter blades	7	-
Number of stator vanes	9	-
Evaporator pressure	0.6	bar(a)
Condenser pressure	2.07	bar(a)
Evaporator saturation temperature	5.1	°C
Condenser saturation temperature	38.7	°C

TABLE 1: DESIGN CONDITIONS OF THE CHILLER AND COMPRESSOR CHARACTERISTICS [10]

A simplified P&I diagram indicating the quantities used in the model is shown in FIGURE 4 [9] and the actual test rig is shown in FIGURE 5 [9]. The compressor is of radial type with bladed diffuser, and its characteristic map, obtained through experiments, is reported in FIGURE 6 [10]. The surge line denoted in FIGURE 6 is the locus of the last stable point for each iso-speed.

Since the test rig did not include a mass flow meter to directly measure the refrigerant mass flow rate at the time of these experiments, it is calculated using enthalpy balance in the heat exchangers [9,10] . TABLE 1 shows the main design features of the chiller, and maximum compressor performance predicted at design point. The refrigerant fluid is R1233zd-(E) [9,10,16], being a modern fluid with low Global Warming Potential and used in low pressure applications. As seen from TABLE 1, at design conditions the evaporator pressure is sub-atmospheric.

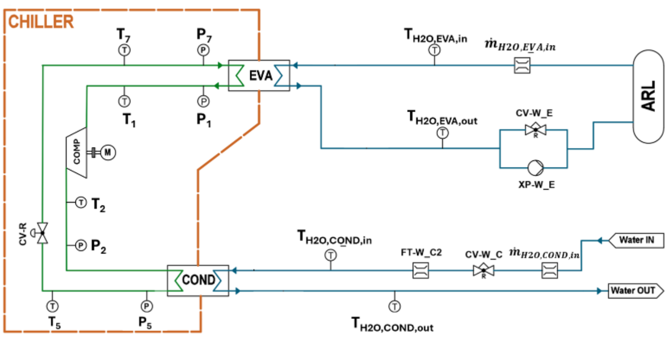

FIGURE 4: SIMPLIFIED P&I DIAGRAM OF TEST RIG [9]

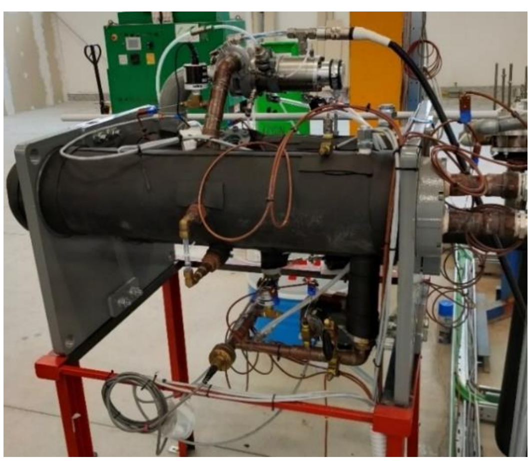

FIGURE 5: EXPERIMENTAL TEST RIG [9]

During plant operation, the compressor is moved from the stable region to stall or surge by operating on the expansion valve opening (CV-R in FIGURE 4). By reducing its opening, the compressor operating point moves to lower mass flow conditions, i.e. reduces surge margin, until stall occurs [10]. Another strategy, not employed for the experimental results in this paper and currently being explored successfully in experiments, is to increase the cooling water temperature sent to the condenser in order to increase its inlet saturation pressure until compressor instabilities begin.

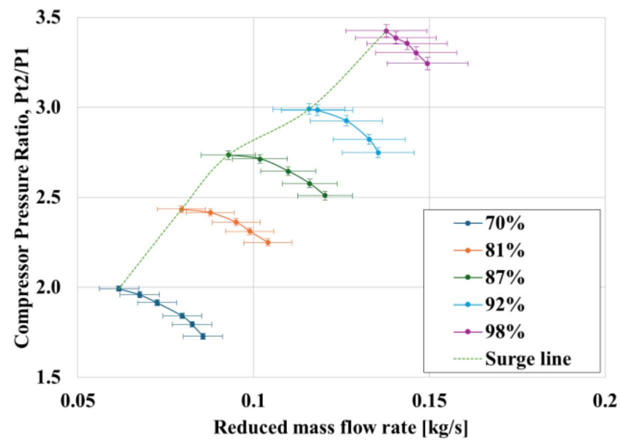

FIGURE 6: COMPRESSOR CHARACTERISTICS MAP [9]

Since the transient model explained here targets the reproduction of mass flow fluctuations in the system and not the complex fluid dynamic behavior inside the compressor such as development of stall cell and flow separation, the experimental results used to validate the model refer to the low frequency compressor surge cycles, while prediction of incipient surge precursors or rotating stall are out of scope of the present work. High frequency experimental data are analyzed in a companion paper [17].

4. RESULTS AND DISCUSSION

The compression system model is simulated for two iso-speed line operations in post stall condition: (i) 92% speed with 14% expansion valve opening and (ii) 87% speed with 14% expansion valve opening. Such iso-speeds are reduced values according to similitude theory and, therefore, may correspond to variable angular speeds of compressor impeller, which is adjusted based on the compressor inlet temperature for constant reduced speed.

The governing equations (1) – (3) & (6) – (9) are solved using the 4th order Runge-Kutta method. The initial conditions are taken as the last stable point of the selected iso-speed line. Since the model does not include the expansion valve, the alternative approach mentioned before is used, where the water temperatures at condenser and evaporator inlets are changed by a small amount (e.g. 1 degree Celsius increase and decrease respectively) until permanent surge cycles are established. The model parameters at the last stable point in the compressor operating curve (FIGURE 6) are mentioned in TABLE 2, with effective volume of heat exchangers tuned to match the real operating conditions.

Test Name	87_19_14	92_19_14
L_{eq}(m)	0.5258	0.5258
A_{eq}(m^2)	7.203x10^{-4}	7.203x10^{-4}
R_m (m)	0.0114	0.0114
Reduced Speed	87%	92%
N_R	2	2
$C_p{}^*{}_{EVA}$	1264.40	1363.10
$C_p{}^*{}_{COND}$	2000.33	2557.60
$C_{V,EVA}$	875.028	875.060
$C_{V,COND}$	878.342	878.478
$V_{effective,EVA}$	0.00395	0.00395
$V_{effective,COND}$	0.001725	0.00184
$T_{H2O,EVA,in}$	291.86	292.00
$T_{H2O,COND,in}$	296.11	296.66
$\dot{m}_{H2O,EVA,in}$	0.9162	0.9278
$\dot{m}_{H2O,COND,IN}$	1.2329	1.2104

TABLE 2: MODEL PARAMETERS

The simulation results show that with the initial conditions of the system set at the last stable point, the change in water circuit temperature pushes the system into instability. From FIGURE 7 and FIGURE 11, it can be seen that the system enters a deep surge event with flow reversal. This event is seen in FIGURE 8 (a) and FIGURE 12 (a) as well.

From the experiment data used for validation of this model, it was not possible to verify this phenomenon as the mass flow, shown in FIGURE 8 (b) & FIGURE 12 (b), is not directly measured in the experiment. Instead, the mass flow rate was estimated using enthalpy balance on the heat exchangers and the external water circuit. The use of thermal balance for refrigerant mass flow estimation makes the mass flow measurement response too slow with respect to surge cycle frequency. However, after installation of visual inspection ports on the compressor inlet and outlet ducts, the presence of liquid droplet entrainment (shown in FIGURE 15) allowed to verify, qualitatively, that flow reversal occurs, demonstrating that this system typically undergoes permanent deep surge cycles. Experimental measurement of reverse flow during surge requires specialized probes, which were not installed in the test rig at the time of development of this model.

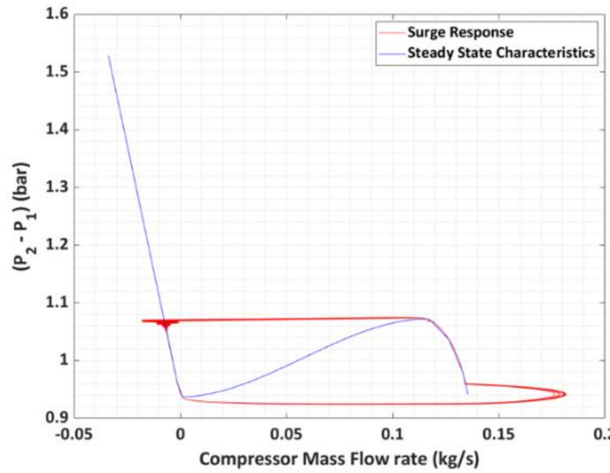

FIGURE 7: SURGE RESPONSE FOR 92% ISO-SPEED

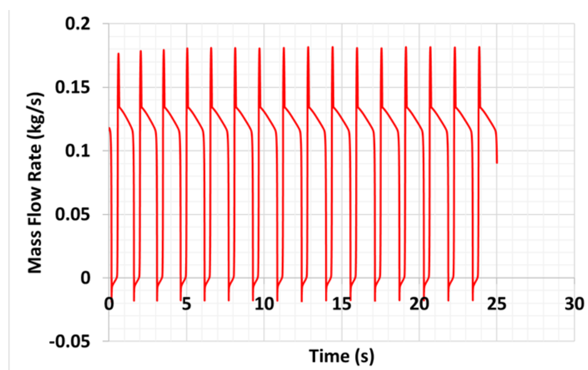

(a)

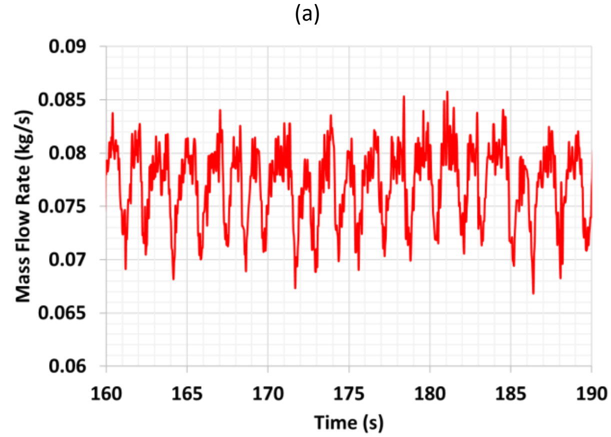

(b)

FIGURE 8: MASS FLOW FLUCTUATION FOR 92% ISO-SPEED (a) MODEL (b) EXPERIMENT

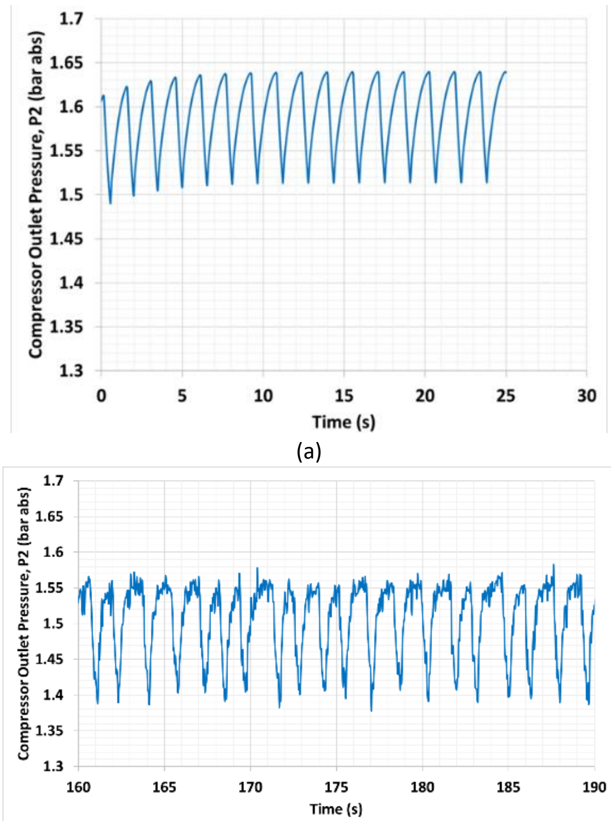

(a)

(b)

FIGURE 9: COMPRESSOR OUTLET PRESSURE FLUCTUATION FOR 92% ISO-SPEED (a) MODEL (b) EXPERIMENT

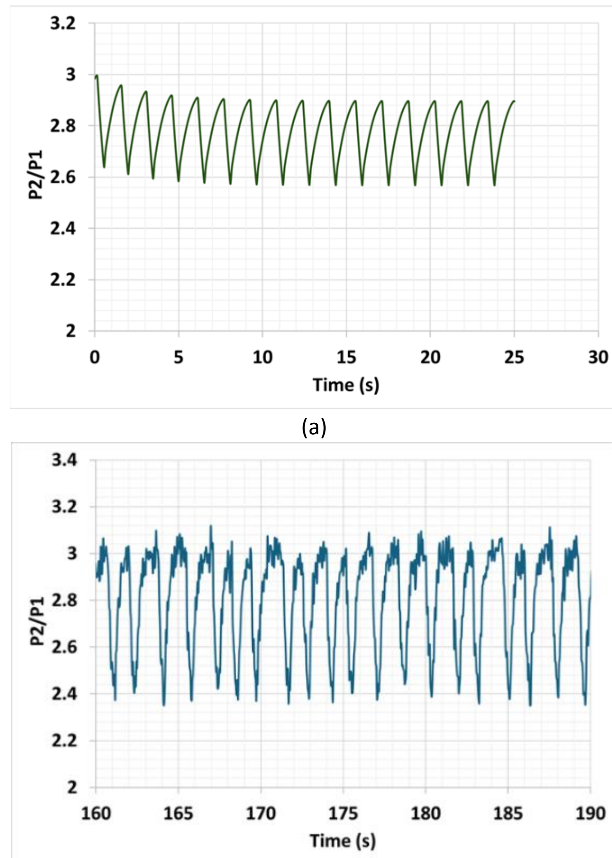

(a)

(b)

FIGURE 10: PRESSURE RATIO FLUCTUATIONS FOR 92% ISO-SPEED (a) MODEL (b) EXPERIMENT

The compressor outlet pressure (P2) is also analyzed, both for the model and the experiment. The results show that the trend in the pressure fluctuations qualitatively match as seen in FIGURE 9 (a) and (b) for 92% iso-speed and in FIGURE 13 (a) and (b) for 87% iso-speed. This is clearly visible in the slow rise followed by sudden drop of the pressure. Furthermore, the static pressure ratio, P_2/P_1, for both the experiment and the simulation, as shown in in FIGURE 10 (a) and (b) for 92% iso-speed and in FIGURE 14 (a) and (b) for 87% iso-speed line, also follows the same shape, representing a qualitative match between the model and the experiment.

The difference between the model and the experiment is also visible both in the average pressure ratio value along the surge cycles, and, at minor extent, in the amplitude of pressure ratio fluctuations. This fact can be explained considering that (i) pressure taps are not immediately placed at the compressor inlet and outlet, and pressure drops occur in between the pressure measurement and the compressor (values are well representative of the heat exchanger pressure), and (ii) the model does not include the dynamics of the refrigerant vapor phase.

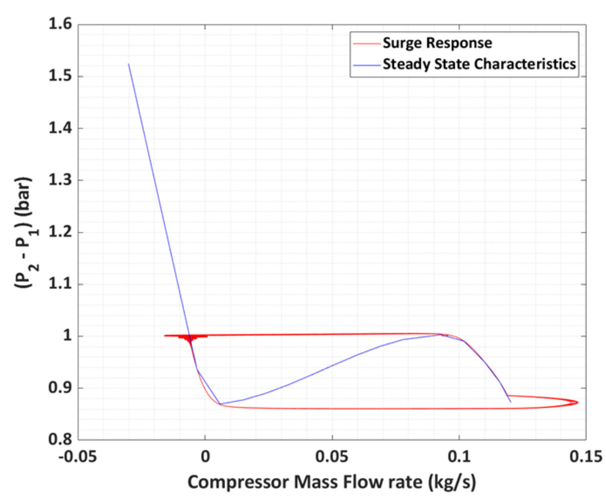

FIGURE 11: SURGE RESPONSE FOR 87% ISO-SPEED

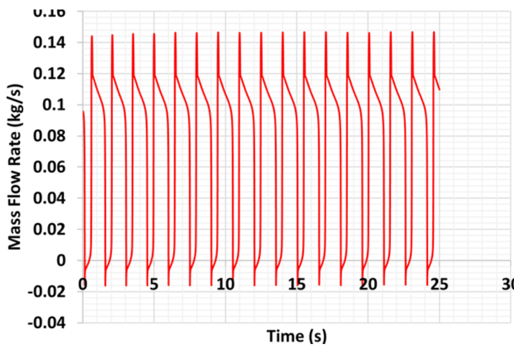

(a)

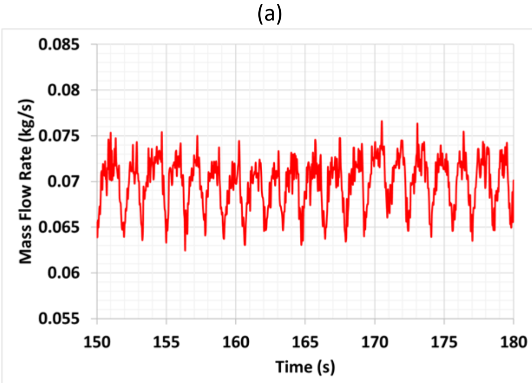

(b)

FIGURE 12: MASS FLOW FLUCTUATION FOR 87% ISO-SPEED (a) MODEL (b) EXPERIMENT

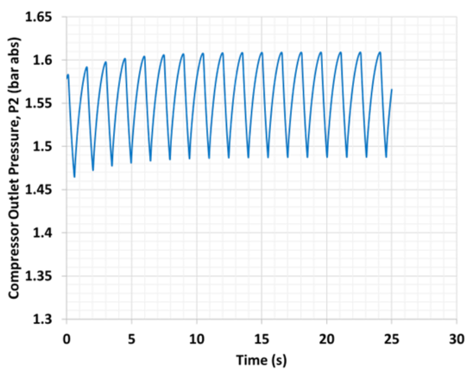

(a)

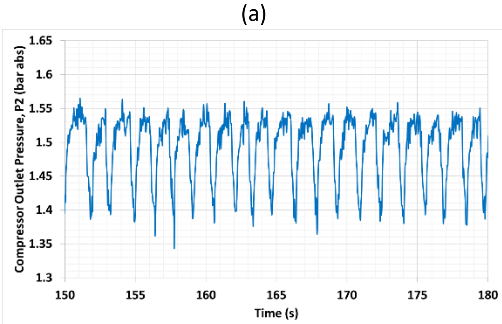

(b)

FIGURE 13: COMPRESSOR OUTLET PRESSURE FLUCTUATION FOR 87% ISO-SPEED (a) MODEL (b) EXPERIMENT

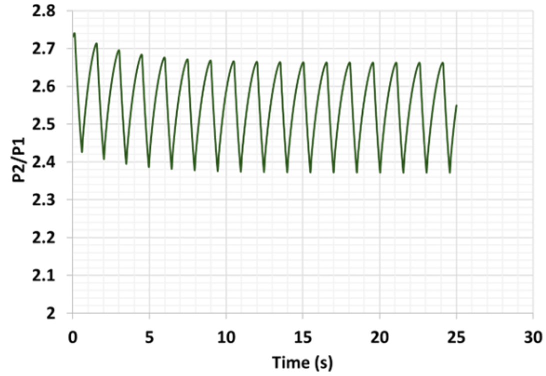

(a)

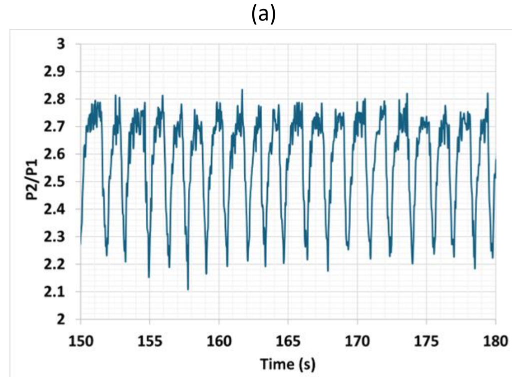

(b)

FIGURE 14: PRESSURE RATIO FLUCTUATIONS FOR 87% ISO-SPEED (a) MODEL (b) EXPERIMENT

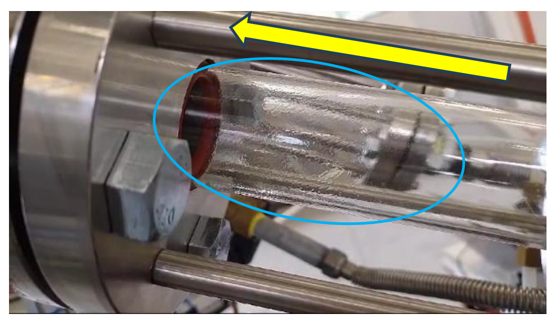

(a)

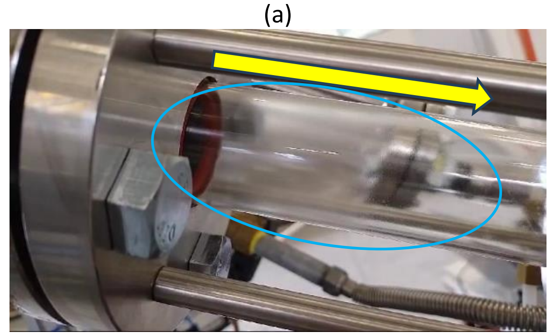

(b)

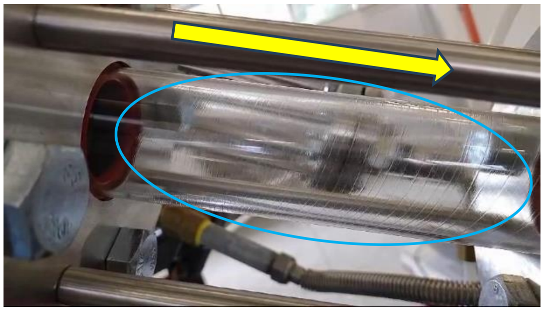

(c)

FIGURE 15: EVIDENCE OF FLOW REVERSAL (a) FORWARD FLOW (b) REVERSE FLOW (c) SPIRAL PATH DURING BACKFLOW.

In FIGURE 15, the behavior of the entrained liquid droplets during forward (FIGURE 15(a)) and reverse flow (FIGURE 15(b)) at compressor inlet is shown. In the reverse flow condition associated with surge event, the distribution of the droplets on the optical window is disturbed by the gases exiting via compressor inlet. Another evidence of reverse flow is seen in FIGURE 15(c), where the droplets form a spiral on the optical window during surge event. This is due to the swirl velocity component imparted by the impeller on the gas, which is flowing out of the compressor inlet.

While pressure measurements allow for a first qualitative verification of the model, because of the relatively low frequency pressure sensors, validation can be performed on the predicted frequency of the surge cycles. From the experimental results for these two cases, the surge frequency was determined on the fluid dynamic measurements and vibroacoustic measurements (FIGURE 16). In surge condition, significant sub-synchronous spectral contents arise which may be due to rotating stall inception, which is modulated in amplitude by surge cycles average frequency. In order to obtain an adequate experimental identification of the low frequency component of surge, a signal demodulation is performed on dynamic structural response obtained through vibroacoustic measurements [17,18].

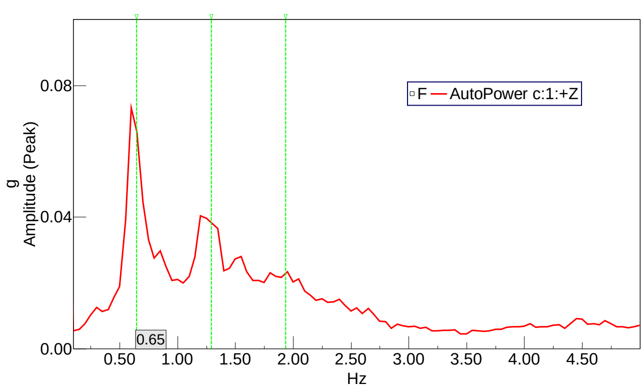

FIGURE 16: LOW FREQUENCY SURGE IDENTIFICATION FROM VIBROACOUSTIC DATA FOR 92% ISO-SPEED

For the model, Fast Fourier Transform on the pressure fluctuations was used to calculate the dominant frequency. The results are listed below in TABLE 3 (test name nomenclature is in accordance with [9,10], reporting percentage speed, evaporator inlet water temperature and expansion valve fractional opening). From TABLE 3, it can be seen that the model predicts the surge frequency quite accurately, not only in absolute values but also in trend. In fact, when the iso-speed moves from 92% down to 87% the surge frequency changes, increasing slightly, in accordance with measurements. This proves that the modelling methodology used is suitable for this type of system, as preliminary approach to surge cycle prediction. The compressor outlet pressure amplitude, shown in TABLE 3, also indicate that the model prediction is close to reality, but there is still room for improvement such as addition of gaseous phase.

Test Name	Speed	Frequency (Hz)		$\frac{(P_{2,max}-P_{2,min})}{P_{2,min}}$ (%)	
		Model	Experiment	Model	Experiment
92_19_14	92%	0.64	0.65	8.32	12.24
87_19_14	87%	0.68	0.67	8.19	12.31

TABLE 3: COMPARISON OF SURGE EVENT WITH EXPERIMENTS

5. CONCLUSION

An initial attempt is made in modelling a two phase, closed loop dynamic compression system for predicting radial compressor post-stall transients. The model is relatively simple, despite based on real geometrical data, and equipped with empirical correlations to capture the complex phenomenon associated with heat exchangers using real fluids. The model results are matched with experimental surge frequencies and qualitatively with the pressure fluctuations during surge. Improvements to the model such as detailed modelling of liquid and gas phases within heat exchangers, inclusion of heat exchanger liquid level data, and addition of thermal capacitance of heat exchanger pipes are planned for the next steps of this research work.

ACKNOWLEDGEMENTS

This project has received partial funding from the European Union's Horizon 2020 research and innovation programme under the Marie Skłodowska-Curie grant agreement No: INSPIRE-956803.

REFERENCES

[1] Baggio, P., Bee, E., and Prada, A., 2018, "Demand-Side Management of Air-Source Heat Pump and Photovoltaic Systems for Heating Applications in the Italian Context," Environments - MDPI, **5**(12). https://doi.org/10.3390/environments5120132.

[2] Rinaldi, A., Soini, M. C., Streicher, K., Patel, M. K., and Parra, D., 2021, “Decarbonising Heat with Optimal PV and Storage Investments: A Detailed Sector Coupling Modelling Framework with Flexible Heat Pump Operation,” Appl Energy, **282**, p. 116110. https://doi.org/10.1016/J.APENERGY.2020.116110.

[3] Song, J., Park, J. C., Kim, K. Y., Jeong, J., and Song, S. J., 2014, “Surge Onset in Turbo Heat Pumps,” J Turbomach, **136**(8). https://doi.org/10.1115/1.4026145.

[4] Marelli, S., Misley, A., and Ferrando, M., 2020, “Experimental Investigation in Turbocharger Compressors during Surge Operation,” *Proceedings of the ASME Turbo Expo*. https://doi.org/10.1115/GT2020-15174.

[5] Kim, H. R., and Song, S. J., 2010, “Modeling of Surge Characteristics in Turbo Heat Pumps,” *Proceedings of the ASME Turbo Expo*. https://doi.org/10.1115/GT2010-23342.

[6] Moore, F. K., and Greitzer, E. M., 1986, “A Theory of Post-Stall Transients in Axial Compression Systems: Part 1—Development of Equations,” J Eng Gas Turbine Power, **108**(1). https://doi.org/10.1115/1.3239887.

[7] Greitzer, E. M., and Moore, F. K., 1986, “A Theory of Post-Stall Transients in Axial Compression Systems: Part II—Application,” J Eng Gas Turbine Power, **108**(2). https://doi.org/10.1115/1.3239893.

[8] Botha, B. W., Du Toit, B., and Rousseau, P. G., 2003, “Development of a Mathematical Compressor Model to Predict Surge in a Closed Loop Brayton Cycle,” *American Society of Mechanical Engineers, International Gas Turbine Institute, Turbo Expo (Publication) IGTI*. https://doi.org/10.1115/GT2003-38795.

[9] Ferrando, M., Reboli, T., Purushothaman, S., Traverso, A., and Halbe, C., 2023, “A New Experimental Test Rig for Performance Analysis of Radial Compressors inside Innovative Heat Pumps,” *Journal of Physics: Conference Series*. https://doi.org/10.1088/1742-6596/2511/1/012003.

[10] Ferrando, M., Reboli, T., Reggio, F., Niccolini Marmont Du Haut Champ, C. A., Silvestri, P., Traverso, A., and Sishtla, V., 2023, “Centrifugal Compressor Surge In Innovative Heat Pump - Part 1: Fluid Dynamic And Vibrational Analysis,” J Eng Gas Turbine Power, pp. 1–14. https://doi.org/10.1115/1.4063547.

[11] Traverso, A., 2005, “TRANSEO Code for the Dynamic Performance Simulation of Micro Gas Turbine Cycles,” *Proceedings of the ASME Turbo Expo*. https://doi.org/10.1115/GT2005-68101.

[12] Traverso, A., Massardo, A. F., and Scarpellini, R., 2006, “Externally Fired Micro-Gas Turbine: Modelling and Experimental Performance,” Appl Therm Eng, **26**(16). https://doi.org/10.1016/j.applthermaleng.2006.01.013.

[13] Mantelli, L., Ferrari, M. L., and Traverso, A., 2021, “Dynamics and Control of a Turbocharged Solid Oxide Fuel Cell System,” Appl Therm Eng, **191**, p. 116862. https://doi.org/10.1016/J.APPLTHERMALENG.2021.116862.

[14] Lambruschini, F., Liese, E., Zitney, S. E., and Traverso, A., 2016, “Dynamic Model of a 10 Mw Supercritical CO2 Recompression Brayton Cycle,” *Proceedings of the ASME Turbo Expo*. https://doi.org/10.1115/GT2016-56459.

[15] Huber, M. L., Lemmon, E. W., Bell, I. H., and McLinden, M. O., 2022, “The NIST REFPROP Database for Highly Accurate Properties of Industrially Important Fluids,” Ind Eng Chem Res, **61**(42). https://doi.org/10.1021/acs.iecr.2c01427.

[16] Mondejár, M. E., McLinden, M. O., and Lemmon, E. W., 2015, “Thermodynamic Properties of Trans-1-Chloro-3,3,3-Trifluoropropene (R1233zd(E)): Vapor Pressure, (p, ρ, T) Behavior, and Speed of Sound Measurements, and Equation of State,” J. Chem. Eng. Data, **60**, pp. 2477–2489.

[17] Niccolini, C. A., Silvestri, P., Reggio, F., Traverso, A., and Sishtla, V., 2024, “Compressor Surge Identification in Innovative Heat-Pump Systems Equipped by Vaned Diffuser Centrifugal Compressor,” GT2024-125074, ASME Turbo Expo 2024 (submitted).

[18] Niccolini Marmont Du Haut Champ, C. A., Silvestri, P., Ferrari, M. L., and Massardo, A. F., 2020, “Signal Processing Techniques to Detect Centrifugal Compressors Instabilities in Large Volume Power Plants,” J Eng Gas Turbine Power, **142**(12). https://doi.org/10.1115/1.4048910.